sustainability

MDPI

Article

Machine Learning Models for the Prediction of the Compressive Strength of Self-Compacting Concrete Incorporating Incinerated Bio-Medical Waste Ash

Nahushananda Chakravarthy H G [1], Karthik M Seenappa [1], Sujay Raghavendra Naganna [2,*] and Dayananda Pruthviraja [3,*]

[1] Department of Civil Engineering, Siddaganga Institute of Technology, Tumakuru 572103, India
[2] Department of Civil Engineering, Manipal Institute of Technology Bengaluru, Manipal Academy of Higher Education, Manipal 576104, India
[3] Department of Information Technology, Manipal Institute of Technology Bengaluru, Manipal Academy of Higher Education, Manipal 576104, India
* Correspondence: sujay.n@manipal.edu (S.R.N.); dayananda.p@manipal.edu (D.P.)

Abstract: Self-compacting concrete (SCC) is a special form of high-performance concrete that is highly efficient in its filling, flowing, and passing abilities. In this study, an attempt has been made to model the compressive strength (CS) of SCC mixes using machine-learning approaches. The SCC mixes were designed considering lightweight expandable clay aggregate (LECA) as a partial replacement for coarse aggregate; ground granulated blast-furnace slag (GGBS) as a partial replacement for binding material (cement); and incinerated bio-medical waste ash (IBMWA) as a partial replacement for fine aggregate. LECA, GGBS, and IBMWA were replaced with coarse aggregate, cement, and fine aggregate, respectively at different substitution levels of 10%, 20%, and 30%. M30-grade SCC mixes were designed for two different water/binder ratios—0.40 and 0.45—and the CS of the SCC mixes was experimentally determined along with the fresh state properties assessed by slump-flow, L-box, J-ring, and V-funnel tests. The CS of the SCC mixes obtained from the experimental analysis was considered for machine learning (ML)-based modeling using paradigms such as artificial neural networks (ANN), gradient tree boosting (GTB), and CatBoost Regressor (CBR). The ML models were developed considering the compressive strength of SCC as the target parameter. The quantities of materials (in terms of %), water-to-binder ratio, and density of the SCC specimens were used as input variables to simulate the ML models. The results from the experimental analysis show that the optimum replacement percentages for cement, coarse, and fine aggregates were 30%, 10%, and 20%, respectively. The ML models were successful in modeling the compressive strength of SCC mixes with higher accuracy and the least errors. The CBR model performed relatively better than the other two ML models, with relatively higher efficiency (KGE = 0.9671) and the least error (mean absolute error = 0.52 MPa) during the testing phase.

Keywords: self-compacting concrete; gradient tree boosting; CatBoost Regressor; incinerated bio-medical waste ash; lightweight expandable clay aggregate (LECA)

check for updates

Citation: Chakravarthy H G, N.; Seenappa, K.M.; Naganna, S.R.; Pruthviraja, D. Machine Learning Models for the Prediction of the Compressive Strength of Self-Compacting Concrete Incorporating Incinerated Bio-Medical Waste Ash. *Sustainability* **2023**, *15*, 13621. https://doi.org/10.3390/su151813621

Academic Editors: Malindu Sandanayake and Ehsan Yaghoubi

Received: 11 August 2023
Revised: 6 September 2023
Accepted: 10 September 2023
Published: 12 September 2023

Copyright: © 2023 by the authors. Licensee MDPI, Basel, Switzerland. This article is an open access article distributed under the terms and conditions of the Creative Commons Attribution (CC BY) license (https://creativecommons.org/licenses/by/4.0/).

1. Introduction

Self-compacting concrete has been used in a variety of civil engineering applications because of its superior flowability, mechanical strength, and durability [1,2]. It has greater application in the areas of underwater concreting; structural members involving heavy reinforcement; solving unskilled labor issues in the construction sector; eliminating the need for vibration; and reducing construction time, labor costs, and noise pollution [3,4]. Generally, SCC consists of a high volume of cement with a low volume of coarse aggregate, and a superplasticizer is used to reduce the water–binder ratio. Environmental and working conditions have substantially improved because of the development of SCC, since there is

lower energy consumption, less vibration, higher productivity, less noise, reduced health hazards, and so on [1,5].

SCC with low density can be produced by partially or completely replacing coarse aggregates with natural or synthetic lightweight aggregates. Lightweight expanded clay aggregate (LECA) is a versatile porous ceramic material manufactured by firing the natural mining clay in a rotary kiln. LECA is utilized in a vast array of applications, including hydroponics, geotechnical fillers, lightweight concrete, and thermal and acoustic insulation. A plethora of microscopic air-filled voids accounts for LECA's lightweight, thermal, and acoustic isolation properties [6,7]. Compared with other kinds of lightweight aggregates, such as pumice, scoria, perlite, etc., LECA can provide a smoother concrete surface. LECA pretreatment with cement and silica fume paste provides it with the requisite qualities for SCC since aggregate strength has the greatest influence on the compressive strength of concrete and LECA has less aggregate strength [8,9].

Currently, several cement substitutes are employed, notably including fly ash, ground granulated blast-furnace slag (GGBS), and metakaolin. The properties of waste materials can vary widely, which can make it difficult to design and produce SCC with consistent properties [10,11]. GGBS is a non-metallic byproduct consisting of aluminosilicates and calcium silicates that are acquired in a molten state with iron in a blast furnace [12–14]. GGBS has the potential to improve both the fresh and hardened qualities of SCC while also promoting sustainability. GGBS delays the setting time of concrete, resulting in an increase in strength over time. Concrete-containing GGBS can reduce heat generation during the hydration process while also improving resistance to sulphate attacks, making it suitable for marine construction [15,16]. Oner et al. (2007) [17], upon investigation of 32 distinct SCC mixes containing GGBS, discovered that when GGBS content increases, the water-to-binder ratio tends to decrease for the same consistency, demonstrating that GGBS has a positive effect on consistency. The CS of concrete mixtures containing GGBS likewise increased substantially as the quantity of GGBS replacement increased. Research by Leelavathi et al. (2021) [18] explored the potential of GGBS as a cement substitute in the production of SCC at 10, 20, 30, 40, and 50% by weight of cement. SCC substituted with 20% GGBS was accepted as an optimal concrete mix compared with other proportions. The addition of GGBS increases the paste volume, which reduces the friction between the paste and the aggregate particles, thus improving the fluidity of the mix.

By replacing concrete constituents with less expensive, recycled, or more sustainable materials, environmental impacts can be minimized. The use of waste materials in SCC is a promising way to reduce the environmental impact of concrete production [19,20]. Biomedical waste poses a significant environmental problem among many other types of waste simply because it is potentially hazardous. The waste produced by hospitals, diagnostic centers, and biological laboratories is collectively called biomedical waste. Incineration is the ideal treatment option for biomedical waste, despite the fact that alternative techniques such as carbon filtration, chemical coagulation, biological oxidation, membrane filtering, and others have been utilized to address this hazardous waste [21,22]. The type of ash emitted and stockpiled in such waste incineration facilities is known as incinerator biomedical waste ash (IBMWA). IBMWA is typically disposed of in landfill to prevent it from spreading into the environment. However, several studies demonstrate the potential for using it to fabricate building materials like bricks, mortar, concrete, asphalt, etc. [23–25]. Aubert et al. (2004) [23] explored the application of IBMWA as a substitute for fine aggregate in concrete production. The durability and CS of hardened concrete were unaffected by the utilization of IBMWA as a supplementary material in concrete [26].

In general, the CS of SCC is determined through physical experimentation, which is expensive and time-consuming. Recent technological innovations have made it possible to handle such engineering problems using alternate methods, which include numerical simulation, empirical regression, and the use of machine-learning (ML) techniques. The prediction of the CS of SCC, in particular, could be addressed by the development of regression models based on machine learning, using specific paradigms that can learn from the input

data and offer extremely precise results. Several ML approaches, including neural networks, ensemble methods, and generalized additive models are used to forecast the compressive strength of SCC [27,28]. Research on the use of neural networks to forecast the compressive strength of various types of concrete mixes began at the end of the 1990s, and neural networks have proven to be quite successful in doing so [29,30]. Since a substantial body of research on the application of several machine-learning paradigms to estimate/predict the compressive strength of different types of concrete exists, it was thought prudent to present a review of some recent literature related to SCC. In a study by Asteris et al. (2016) [31], multilayer feed-forward neural networks predicted the 28-day CS of admixture-based SCC with low significant error rates and computational cost. Likewise, Yaman et al. (2017) [32] applied multi-input–multi-output neural network models for predicting SCC's ingredients (model outputs) based on its hardened and fresh properties (model inputs). A hybrid model that includes a beetle antennae search (BAS) algorithm with a random forest (RF) was developed by Zhang et al. (2019) [33] to predict the uniaxial compressive strength of lightweight SCC. The predictive capabilities of genetic programming (GP) and artificial neural networks (ANN) were comparatively evaluated by Awoyera et al. (2020) [34] to estimate the strength properties of geopolymer SCC with mineral admixtures. Similarly, Farooq et al. (2021) [35] modeled the CS of SCC modified with fly ash by implementing support-vector-machine (SVM), ANN, and gene-expression-programming (GEP) methods. Based on experimental datasets gathered from prior studies, recent research by Hoang (2022) [36] employed Levenberg–Marquardt artificial neural networks (LM-ANN), genetic programming (GEP), deep neural network regression (DNNR), support vector regression (SVR), extreme gradient boosting machines (XGBoost), adaptive boosting machines (AdaBoost), and gradient boosting machines (GBM) to predict the CS of SCC. The DNNR model outperformed the other models in his tests for predicting the CS of SCC. In recent times, novel ensemble methods and hybrid ML approaches have been intensively investigated for predicting the compressive strength of SCC [28,37] and in other domains of structural and transportation engineering [38,39].

The current research was conducted in two phases. In the experimental phase, GGBS, IBMWA, and LECA were substituted for cement, fine aggregate, and coarse aggregate, respectively, in quantities ranging from 10% to 30% by weight, with a 10% increment. To produce SCC, two different water-to-binder ratios—0.4 and 0.45—were adopted. The mix designs comprise permutations and combinations of various material substitutions. In the second phase, machine-learning models were developed for simulating the CS of the SCC produced. Extensive effort was expended in compiling experimental data (384 samples), which was then used for modeling. To the best of the authors' knowledge, only limited research has been undertaken on ML modeling of the compressive strength of SCC. For the first time, the CS of SCC produced by blending GGBS, IBMWA, and LECA is modeled utilizing the most recent ML techniques, such as gradient tree boosting and CatBoost Regression.

2. Materials

The self-compacting concrete mixtures produced comprised fine aggregate, coarse aggregate, cement as the binding agent, GGBS as a supplementary cementitious material, superplasticizers, and IBMWA and LECA as aggregate replacement materials.

2.1. Cement

For all design mix proportions, ordinary Portland cement (Zuari brand) of grade 43, in compliance with IS:8112-1989 (2013) [40], was used. The grey cement was free from hard lumps. Basic tests, such as final setting time, initial setting time, specific gravity, and normal consistency tests were conducted. The cement was tested in accordance with Bureau of Indian Standards codal provisions, and the results provided by the manufacturer were verified with the specifications mentioned in IS:8112-1989 (2013). The test results for the physical properties of cement are tabulated in Table 1.

Table 1. Physical properties of cement.

Tests Conducted	Results Obtained
Normal consistency (%)	30%
Specific gravity	3.13
Initial setting time (minutes)	65
Final setting time (minutes)	380
Fineness	
Dry sieving (%)	2.39
Blains air permeability value (m^2/kg)	287
Soundness	
Le Chatelier value (mm)	1.2
Autoclave (%)	0.076
Compressive Strength, (MPa)	
At 3 days	27.84
At 7 days	37.33
At 28 days	48.28

2.2. Aggregates

Locally available crushed-granite gravel (20 mm downsize) was used as the coarse aggregate in the experimental work. According to the codal provisions of the Bureau of Indian Standards, the physical properties of the coarse aggregate, notably specific gravity, fineness modulus, bulk density, and water absorption, were determined. The test results are presented in Table 2. Likewise, locally available manufactured sand (M-Sand) was used as the fine aggregate, with the particle size distribution adhering to the zone II grading cited in Table 4 of IS:383-1970 (2002) [41]. The physical properties of the fine aggregate were determined and are tabulated in Table 3.

Table 2. Physical properties of the coarse aggregate.

Tests	Results
Specific gravity	2.64
Water absorption (%)	0.8
Particle size	20 mm and down
Fineness modulus	6.02
Bulk density (kg/m^3)	1511

Table 3. Physical properties of the fine aggregate (M-Sand).

Tests	Results
Specific gravity	2.60
Gradation	Zone II
Particle size	4.75 mm and down
Water absorption (%)	1.8
Bulk density (kg/m^3)	1699.65

2.3. Lightweight Expandable Clay Aggregate (LECA)

LECA is a lightweight porous ceramic aggregate manufactured by firing clay to about 1200 °C in a rotary kiln. The LECA used in this research (Figure 1) was procured from Gujarat, India. The properties of LECA, particularly specific gravity, water absorption, and bulk density were determined, and the results are reported in Table 4.

LECA particles become the primary source of weakness in concrete if used directly without pre-treatment. The pre-treatment method endorsed should be capable of strengthening them. In this study, LECA was given a pre-treatment that involved soaking it in water for 24 h and letting the surface air-dry on its own. Soon after that, the dried LECA was

then soaked in cement paste. After being thoroughly coated with cement paste for 5 min, the surface-dried LECA particles were then removed from the paste with a screen/sieve and left to air-dry at room temperature. The LECA particles were wrapped and stored once the paste had completely dried out to keep them moist. The cement paste had a water-to-binder ratio of 0.6. The steps involved in pre-treatment are illustrated in Figure 2.



Figure 1. The LECA aggregate.

Table 4. Physical properties of LECA.

Tests	Results
Specific gravity	1.38
Water absorption (%)	30%
Particle size	20 mm and down
Bulk density (kg/m^3)	495

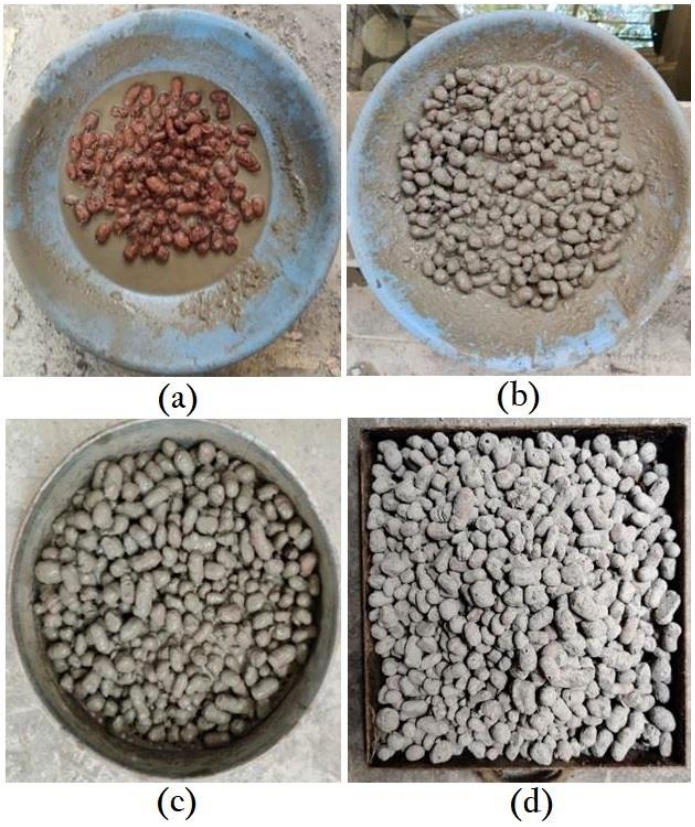


Figure 2. (**a**) Addition of LECA to the paste, (**b**) mixing LECA with the paste, (**c**) removing LECA from the paste, (**d**) air-dried and cured LECA.

2.4. Ground Granulated Blast Furnace Slag (GGBS)

The GGBS used in this study (Figure 3) was fetched from SD Conmix, a construction firm in Karnataka. Its properties, such as specific gravity, bulk density, and fineness were determined, and the results are tabulated in Table 5.



Figure 3. GGBS sample.

Table 5. Physical properties of GGBS.

Tests	Results
Specific gravity	2.92
Colour	Off-White
Bulk density (kg/m^3)	1050
Fineness (m^2/kg)	372

2.5. Incinerated Bio-Medical Waste Ash (IBMWA)

The IBMWA used in this study (Figure 4) was fetched from a bio-medical waste management plant managed by Medicare Environmental Management (P) Ltd. located at Dabaspete, Karnataka. Its properties, notably water absorption, specific gravity, and bulk density were determined, and the results are tabulated in Table 6. The chemical composition of IBMWA ash was analyzed using X-ray fluorescence (PAN Analytical) following the guidelines of IS:12803-1989 [42], and its constituents are reported in Table 7.



Figure 4. IBMWA sample.

Table 6. Physical properties of IBMWA.

Tests	Results
Gradation	Zone III
Water absorption (%)	3.9
Specific gravity	2.54
Bulk density (kg/m^3)	1415

Table 7. Chemical composition of incinerated biomedical waste ash (IBMWA).

Constituents	(%)
SiO_2	12.11
Al_2O_3	7.82
Fe_2O_3	1.98
CaO	17.8
MgO	2.18
Na_2O	3.55
K_2O	1.25
SO_3	9.17
MnO_2	6.85
PbO	4.25
ZnO	12.9
Others	20.14

2.6. Admixture

Plastol Ultraflow® 4000, a superplasticizing admixture of specific gravity 1.1 and chloride content < 0.2%, was used in this study. This admixture was necessary to achieve better workability as the SCC mixes were designed with low water-to-binder ratios.

3. Methodology

3.1. Mix Design

After obtaining the basic test results for the materials, M30-grade SCC was designed as per the IS 10262: 2019 [43] guidelines. GGBS, IBMWA, and LECA were considered for substitution with cement, fine aggregate, and coarse aggregate, respectively, in quantities ranging from 10% to 30% by weight, with a 10% increment. The superplasticizer (SP) (%) was pre-set for two distinct water-to-binder (W/B) ratios; specifically, the 0.4 W/B ratio had 1.4% SP and the 0.45 W/B ratio had 0.6% SP. Mix design codes, such as SCC 0-0-0 (which stands for self-compacting concrete with 0% LECA, 0% GGBS, and 0% IBMWA), were coined for ease of identification. The codes and mix design to produce 1 m^3 volume of SCC are both detailed in Table S1. In a concrete mixer, each SCC mix was thoroughly mixed until a consistent mixture was produced. The fresh mix was poured into a standard 150 mm cube mold without vibration. All casted molds were cured for 28 days in a curing tank before being tested in a compression testing machine.

3.2. Experimental Testing

3.2.1. Fresh Properties of Concrete

The workability of self-compacting concrete was evaluated with four tests: slump flow, J-ring, L-box, and V-funnel.

- Slump flow

This is one of the most widely used tests and provides an accurate assessment of the filling ability of SCC. In the absence of barriers, slump flow is utilized to evaluate the horizontal free flow of SCC. The test technique is based on the approach used to determine slump. The diameter of the concentric spread of concrete serves as a measure of the concrete's filling capacity. However, it does not indicate the concrete's capacity to move

between reinforcements without being blocked. The slump flowability of SCC is shown in Figure 5a.



Figure 5. (**a**) Slump flow test; (**b**) J-ring test; (**c**) V-funnel test; (**d**) L-box test.

- J-Ring

In this test, the SCC sample is allowed to flow/spread in all directions while being restrained by a circular arrangement of reinforcing bars. The flow is solely produced by gravity in basic setup, such as that recommended by European standards. Due to the blocking effect of the reinforcement bars, the SCC's limited deformability is reflected by the J-ring flow spread, and the flow time shows the rate of spread within a specified flow distance. The J-ring flowability of SCC is shown in Figure 5b.

- V-funnel

The V-funnel test is conducted to evaluate the filling ability of SCC with a maximum aggregate size of 20 mm. The V-funnel test measures the ease of flow of concrete; a shorter flow time indicates greater flowability. The V-funnel is filled with 12 L of concrete, and the time it takes for the concrete to flow through the V-funnel is measured. The funnel may then be loaded with concrete and placed aside for 5 min to set. If the concrete segregates, the flow time, which is slightly correlated with the plastic viscosity of SCC, will be significantly increased. V-funnel passing ability is shown in Figure 5c.

- L-Box

An L-shaped shaped box with vertical and horizontal chambers that are separated by a moveable gate, and in front of which vertical reinforcement bars are mounted, was used in this experimental study. After pouring concrete into the vertical portion, the gate is raised to allow concrete to flow into the horizontal area. The fraction of the level of the concrete at the end of the horizontal portion and the level that remains in the vertical part after the flow ceases are taken into account. This reflects the resting slope of the concrete.

This test measures passing ability or the amount of concrete that can travel between the bars. L-box passing ability is shown in Figure 5d.

3.2.2. Hardened Properties of Concrete

The compressive strength of 28-day-cured cubes was determined. Concrete's compressive strength is one of its primary mechanical properties. The compressive strength measured in megapascals is computed by dividing the ultimate load withstood by the cube's cross-sectional area.

3.3. Theoretical Overview

3.3.1. Artificial Neural Networks (ANN)

Among a variety of machine-learning techniques, ANN always stands out among others in estimating, approximating, or predicting tasks owing to its capability of data mining from supervised learning using an empirical risk minimization framework. In the present study, a multilayer perceptron (MLP) network based on a backpropagation learning strategy was considered. The MLP network comprised three layers: an input layer (with six input parameters), hidden layer, and output layer (with one parameter). Based on trial and error, the ideal number of nodes in the hidden layer was adjusted. Each node-to-node connection was assigned weights fine-tuned to minimize the loss function using the optimization algorithm termed the Levenberg–Marquardt optimization. Tansig, logsig, and purelin were the activation functions employed. The MLP network with the lowest RMSE and highest correlation coefficient during the testing phase was considered to be the optimal network [44,45]. For further information on the ANN algorithm, its various structures, network optimization, and so forth, refer to the following literature [46,47].

3.3.2. Gradient Tree Boosting (GTB)

Friedman [48] introduced the gradient-tree-boosting (GTB) model, which is an iterative decision tree algorithm that takes into account the regression trees (weak/base learners) that are ensembled by gradient boosting. Weak learners are commonly employed in boosting since they get trained faster. To reduce generalization error, weak learners work sequentially in GTB to optimize the bias–variance tradeoff. Each tree tries to improve on the predictive error from the previous tree and uses the computed pseudo-residual as the dependent variable to update the next tree and again determine the new pseudo-residual. By reiterating these steps, the final model is built sequentially by aggregating the activated outputs of each tree with the corresponding boosting weights following a gradient descent approach. In building the GTB regressor, the main parameters used are 'loss' and 'n_estimators'. In this context, 'loss' denotes the value of the loss function that needs to be optimized. The parameter 'n_estimators' determines the number of weak learners. The hyper-parameter labelled 'learning_rate' [in the range (0–1)] avoids overfitting via shrinkage. For further information on the GTB algorithm, stochastic gradient boosting, shrinkage, regularization, tree constraints, and so forth, refer to the following literature [49,50].

3.3.3. CatBoost Regressor (CBR)

CatBoost does, in fact, belong to the family of gradient-boosting decision trees. Cat Boost excels at machine-learning tasks since it implements oblivious decision trees to handle heterogeneous data. CatBoost, unlike other boosting algorithms, includes symmetric trees (balanced trees). In each successive step, the leaves from the prior tree are split using the same criterion. In the whole balanced tree, the feature-split pair with minimal loss (as determined by a penalty function) is picked and applied to all the level's nodes. The CatBoost architecture promotes efficient CPU implementation, reduces prediction time, and regulates overfitting. To prevent overfitting, CatBoost employs the ordered boosting technique, a permutation-driven strategy, to train the model on a subset of the data while computing residuals on a different subset. CatBoost indeed has some common training parameters with GTB but provides a much more flexible interface for fine-tuning parameters.

CatBoost's sensitivity to hyperparameters and their adjustments must be carefully considered in order to build a robust model. For further information on the CatBoost algorithm, its implementation, and so forth, refer to the following literature [51,52].

3.4. Model Development

Machine-learning methods necessitate the division of datasets into training and testing subsets. During model development, the model is calibrated using the training dataset by optimizing its hyperparameters. Finally, the testing dataset is utilized to demonstrate the model's performance in estimation/prediction. The dataset for the current study included 384 samples with six input variables and one output variable. Multivariate regression analysis was implemented; hence, all the SCC constituents were considered input parameters for the model-building process. The input variables include the SCC ingredients LECA (%), GGBS (%), and IBMWA (%); the density of SCC (kg/m^3); water-to-binder (W/B) ratio; and superplasticizer (SP) (%), and the compressive strength (MPa) of the SCC was considered as the output parameter. Knowing that GGBS, IBMWA, and LECA were substituted for cement, fine aggregate, and coarse aggregate, respectively, it is obvious that cement (%) can be computed simply if GGBS (%) is known, and vice versa. Hence, SCC constituents, namely cement (%), fine aggregate (%), and coarse aggregate (%) were excluded as input parameters. The whole dataset was randomly divided into 70% of samples as the training dataset and 30% of samples as testing dataset for the modeling of the CS of SCC. The descriptive statistics of the model parameters are as mentioned in Table 8. Three ML approaches, namely the ANN, GTB, and CBR approaches, were developed in this study to simulate the CS of SCC. The hyperparameters of all the models tuned by the trial-and-error approach during the model development process are presented in Table 9.

Table 8. Descriptive statistics of the SCC dataset.

TRAINING							
	LECA %	**GGBS %**	**IBMWA %**	**DENSITY kg/m^3**	**W/B Ratio**	**SP %**	**CS (MPa)**
MIN	0	0	0	2109.333	0	0.6	18.07
MAX	30	30	30	2530.667	0.45	1.4	39.61778
MEAN	14.92188	15	15	2260.444	0.425	1	27.73663
SDV	11.27177	11.20224	11.20224	92.31112	0.025049	0.400784	4.292255
CV	0.755385	0.746816	0.746816	0.040838	0.058939	0.400784	0.15475
TESTING							
	LECA %	**GGBS %**	**IBMWA %**	**DENSITY kg/m^3**	**W/B Ratio**	**SP %**	**CS (MPa)**
MIN	0	0	0	2114.963	0.4	0.6	18.83
MAX	30	30	30	2486.519	0.45	1.4	39.21
MEAN	14.92188	15	15	2259.845	0.425	1	27.64
SDV	11.29393	11.22427	11.22427	90.72124	0.025098	0.401572	4.3
CV	0.75687	0.748285	0.748285	0.040145	0.059054	0.401572	0.155572

Note: MIN–minimum; MAX–maximum; SDV–standard deviation; CV—coefficient of variation.

3.5. Performance Evaluation

The performance of the developed ML models was evaluated using statistical indices such as mean absolute error (MAE), root-mean-square error (RMSE), Willmot index (WI), Nash–Sutcliffe efficiency (NSE), Kling–Gupta efficiency (KGE), and symmetric mean absolute percentage error (SMAPE). The mathematical formulations of these statistical metrics are presented below:

- Mean absolute error (MAE):

$$MAE = \frac{\sum_{i=1}^{n} |y_i - x_i|}{n} \quad (1)$$

- Root-mean-square error (RMSE):

$$RMSE = \sqrt{\frac{\sum_{i=1}^{n} (x_i - y_i)^2}{n}} \quad (2)$$

- Correlation coefficient:

$$R = \left[\frac{\sum_{i=1}^{n} (x_i - \overline{x})(y_i - \overline{y})}{\sqrt{\sum_{i=1}^{n} (x_i - \overline{x})^2 \sum_{i=1}^{n} (y_i - \overline{y})^2}} \right] \quad (3)$$

- Willmott index:

$$WI = \frac{\sum_{i=1}^{n} (x_i - y_i)^j}{\sum_{i=1}^{n} \left(|y_i - \overline{x_i}| + |x_i - \overline{x_j}| \right)^j} \quad (4)$$

- Nash–Sutcliffe efficiency (NSE)

$$NSE = 1 - \frac{\sum_{i=1}^{n} (x_i - y_i)^2}{\sum_{i=1}^{n} (x_i - \overline{x})^2} \quad (5)$$

- Kling–Gupta efficiency (KGE)

$$\mathrm{KGE} = 1 - \sqrt{(R-1)^2 + (\beta - 1)^2 + (\gamma - 1)^2} \quad (6)$$

R: Correlation coefficient.
β: The ratio of the mean of the simulated values to the mean of the observed data.

$$\beta = \frac{\overline{y}}{\overline{x}} \quad (7)$$

γ: The ratio of the standard deviation of the simulated values to the observed standard deviation.

$$\gamma = \frac{CV_y}{CV_x} = \frac{\frac{\sigma_y}{\overline{y}}}{\frac{\sigma_x}{\overline{x}}} \quad (8)$$

- Symmetric mean absolute percentage error (SMAPE):

$$SMAPE = \frac{100}{n} \sum_{i=1}^{n} \frac{|y_i - x_i|}{(|x_i + y_i|)/2} \ \% \quad (9)$$

where x_i is the observed values, y_i is the model-computed values, $\overline{x}$ is the mean of the observed values, $\overline{y}$ is the mean of the model-computed values, and n is the number of values.

Table 9. Parameter settings used for model building.

Model Parameters	Settings
ANN	
Number of hidden layer neurons	9
Input layer activation function	logsig

Table 9. *Cont.*

Model Parameters	Settings
Output layer activation function	purelin
Epochs	200
GTB	
n_estimators	100
max_depth	9
min_sample_split	9
learning_rate	0.09
loss	Lad *
CBR	
iterations	100
learning_rate	0.2
depth	8

* Note: lad—least absolute deviation.

4. Results and Discussion

4.1. Experimental Results

4.1.1. Fresh Properties

- Slump flow

The diameter of the slump flow is the fundamental fresh property criterion of SCC. The SCC fills the formwork owing to its self-weight to a greater extent if the slump flow (SF) value is higher. In this study, the diameter of the slump flow lies between 660 and 780 mm. According to the standards, the slump flow should lie between 650 and 800 mm, and all the mix designs met this criterion. For 30% replacement of coarse aggregate with LECA, the slump flow was found to be 780 mm for a 0.4 W/B ratio, whereas, for 30% replacement of fine aggregate, coarse aggregate, and cement with IBMWA, LECA, and GGBS, respectively, the slump flow was found to be 660 mm. Slump flow rises as LECA content increases owing to its lightweight properties, whereas slump flow declines with increasing GGBS or incinerated biomedical waste ash as flowability gets reduced due to the paste generated by these two components. Slump flow results for all the SCC mixes are shown in Figure 6.

- V-funnel

The V-funnel test was used to determine the self-compacting concrete's capacity for filling. More flowability is indicated by shorter flow times. For SCC, the flow rate of the concrete through the V-funnel must lie between 6 and 12 s. In this study, the period of flow through the V-funnel lies between 6 and 11 s, which is within the acceptable limit. The V-funnel results for all the SCC mixes are shown in Figure 7. For 30% LECA content, the period of flow through the V-funnel was 7 s, which indicates greater flowability through the section. For 30% GGBS and 10% IBMWA, the time period was 8 s, indicating good flowability properties. However, as IBMWA content increased, the time period also increased, indicating less flowability.

- L-box

The passing ability of SCC can be measured by the L-box test. For self-compacting concrete, the blocking ratio (h2/h1) should lie between 0.8 and 1. The blocking ratio increased and was almost equal to 1 with an increase in LECA content, and it decreased with an increase in GGBS or IBMWA content. The L-box results for all SCC mixes are shown in Figure 8. For 30% LECA content, the blocking ratio was almost equal to 1, due to the high flowability of the SCC mix. Even when provided with 10% GGBS and 10% IBMWA, the blocking ratio was near to 1. A further increase in the replacement with GGBS and IBMWA

decreased the blocking ratio, indicating the blocking effect of the reinforcements. The paste formed in the mix inhibited the flow properties, but it helped with filling the molds.

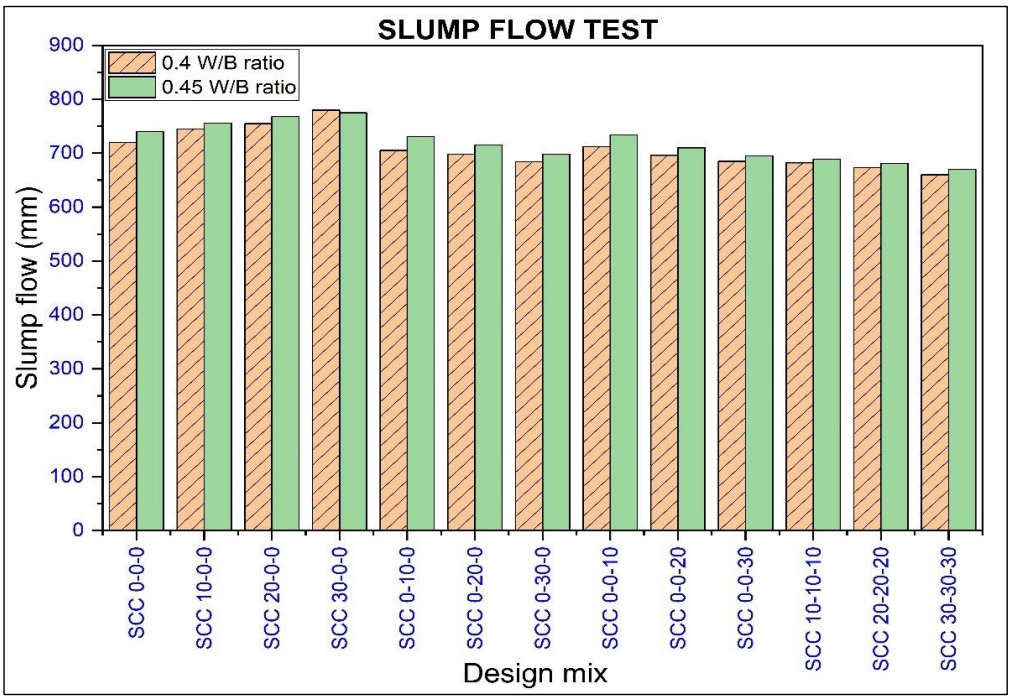


Figure 6. Slump flow test results for SCC with 0.4 and 0.45 W/B ratios.

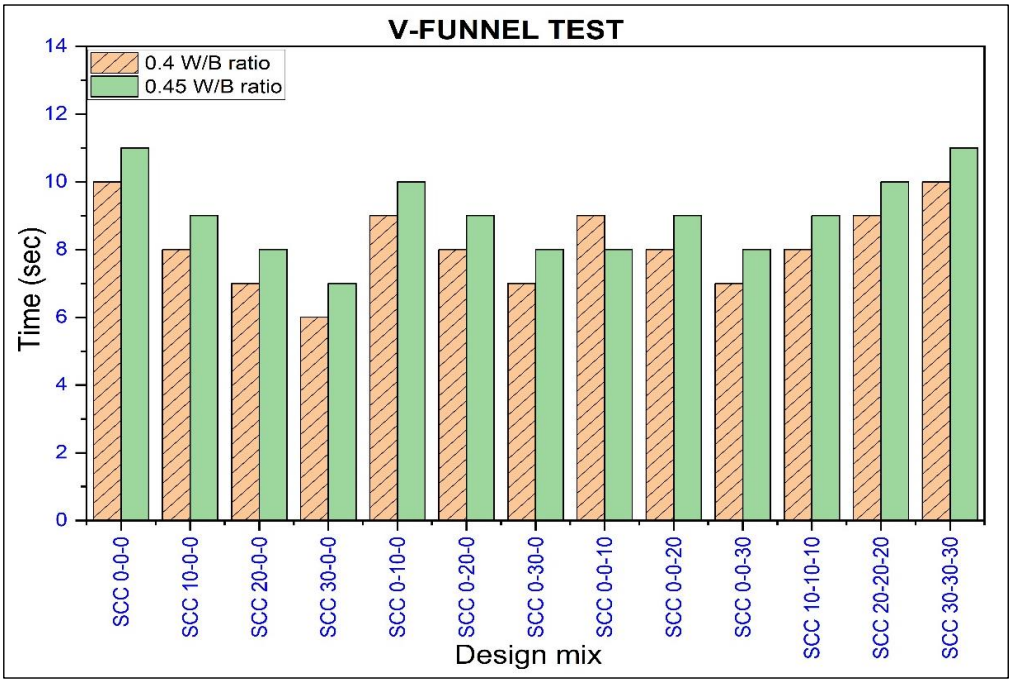


Figure 7. V-funnel test results for SCC with 0.4 and 0.45 W/B ratios.

- J-ring

For self-compacting concrete, the difference in height (between the interior and exterior) of the J-ring must lie between 0 and 10 mm. In this study, the test results for the J-ring ranged from 7 to 10 mm and were within the permissible limit. The smaller the height difference, the greater the flowability and passing ability. The J-ring results for all SCC

mixes are shown in Figure 9. For the mix with 30% GGBS, 30% LECA, and 30% IBMWA content, the difference in height was 10 mm, indicating that flow was restricted between the reinforcements. In addition to having a strong resistance to static segregation, SCC containing GGBS and IBMWA flows without settlement.

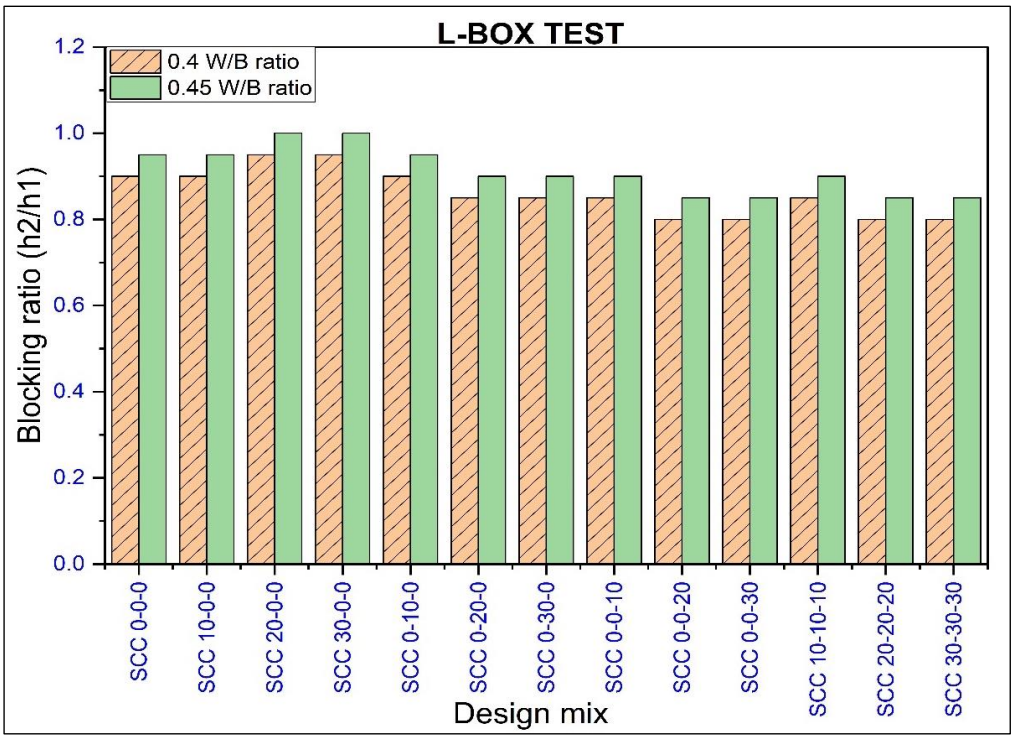


Figure 8. L-box test results for SCC with 0.4 and 0.45 W/B ratios.

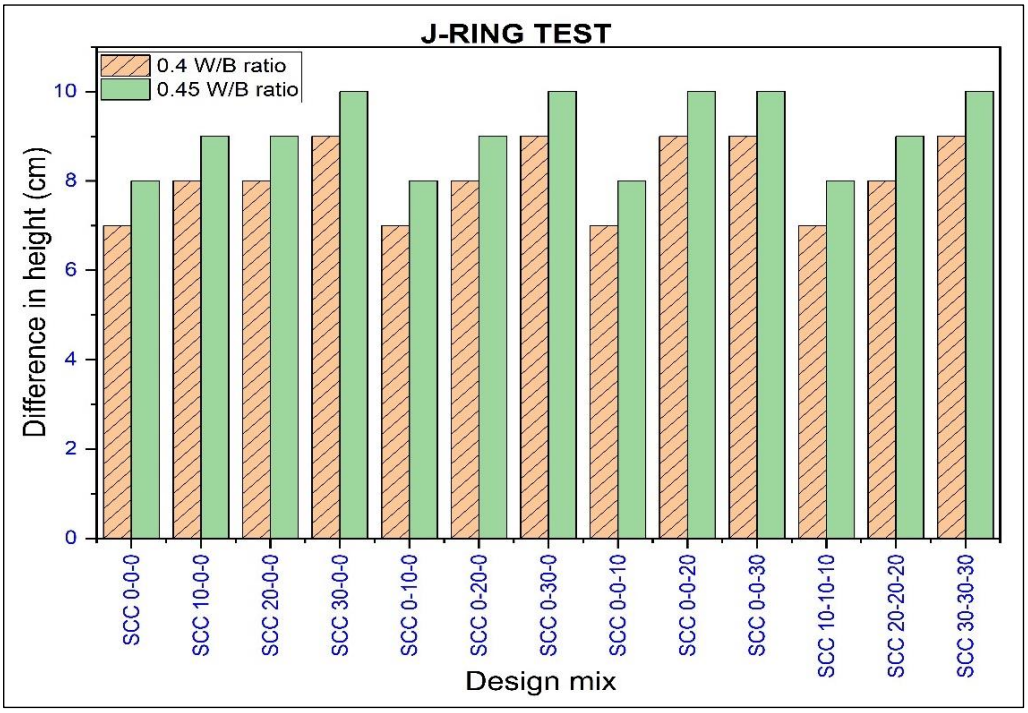


Figure 9. J-ring test results for SCC with 0.4 and 0.45 W/B ratios.

4.1.2. Hardened Properties of SCC Mixes

The cube compressive strength of SCC with the substitution of GGBS, IBMWA, and LECA at various percentages from 0 to 30 with two different water-to-cement ratios of 0.4 and 0.45 were determined experimentally. The obtained results for various percentages of replacement by LECA, GGBS, and IBMWA for 0.4 and 0.45 W/C ratios are presented in Figure 10a and Figure 10b, respectively. At a 0.4 W/B ratio, in the SCC with 10% LECA replacement (SCC 10-0-0), the compressive strength increased by 3.8%, and this is regarded as the optimum LECA replacement percentage. Likewise, at 20% IBMWA replacement of fine aggregate (the SCC 0-0-20 mix), compressive strength increased by 4.6%, and this is the optimum IBMWA replacement percentage. Even though IBMWA raises the water requirement, it is advantageous for the strength of SCC since the high fine content escalates the paste volume. Meanwhile, at 30% replacement of cement with GGBS (the SCC 0-30-0 mix), compressive strength increased by 10.7%, making it the optimum GGBS replacement percentage. Enough literature evidence is available to show that GGBS and IBMWA substitution enhance the hydration process and CSH content, thereby increasing the strength of SCC [12,13,21,24].

Correspondingly, for a 0.45 W/B ratio, at 10% replacement of coarse aggregate with LECA (the SCC 10-0-0 mix), compressive strength increased by 2.8%, and at 10% replacement of fine aggregate with IBMWA (the SCC 0-0-10 mix), compressive strength increased by 2.6%. At 30% replacement of cement with GGBS (the SCC 0-30-0 mix), compressive strength increased by 7.7%, because partially substituting cement with GGBS creates a denser concrete matrix of enhanced strength. The density of SCC mixes decreased with an increase in LECA content. As LECA is a lightweight material, the density varies in accordance with the percentage of replacement. LECA has a lower specific gravity than normal aggregates, which helps reduce the density of the SCC. However, LECA has a higher porosity, which means that it has more voids or pore spaces. These voids may weaken the SCC by reducing the cross-sectional area of the matrix and providing pathways for cracks to propagate.

For a 0.4 W/B ratio, the density of concrete was reduced by 5.5%, 8.5%, and 11% at LECA replacement rates of 10%, 20%, and 30% with coarse aggregates, respectively. Figure 11 depicts the variation in density with % LECA replacement with reference to mixes with a 0.4 W/B ratio. Likewise, for a 0.45 W/B ratio, the density of concrete decreased by 6.6%, 9.6%, and 13% for 10%, 20%, and 30% LECA replacement rates with coarse aggregates, respectively. The variation in density with the % LECA replacement in SCC mixes with a 0.45 W/B ratio is illustrated in Figure 12. The W/B ratio employed, the packing density of the aggregates, and the degree of hydration that takes place within the SCC all affect its density. Since SCC contains less coarse aggregates, a possible drop in density is anticipated. However, the inclusion of GGBS and IBMWA tends to offset this impact in all mixes, and hence there is no noticeable difference in density compared with conventional mixes due to the higher fineness of GGBS and IBMWA, which enhances packing density. The paste volume increases with the inclusion of waste admixtures such as GGBS and IBMWA. The fluidity of the mix gets better as the GGBS dosage rises because the increased paste volume decreases friction between the aggregate and paste particles.

Previous research by Mohamed and Najm (2017) [53] determined that 35% was the optimum GGBS replacement ratio for producing SCC with high compressive strength. Our findings are congruent with theirs, demonstrating that a 30% replacement of cement with GGBS (in the SCC 0-30-0 mix) produced significant strength relative to other mixtures. Similar to this, work by Dolatabad et al. (2021) [54] showed that 15% was the ideal LECA replacement ratio for producing SCC without compromising the strength. Our findings are in line with theirs, where a 10% replacement of coarse aggregates with LECA (in the SCC 10-0-0 mix) provided strength that was comparable to that of the standard (SCC 0-0-0) mix.

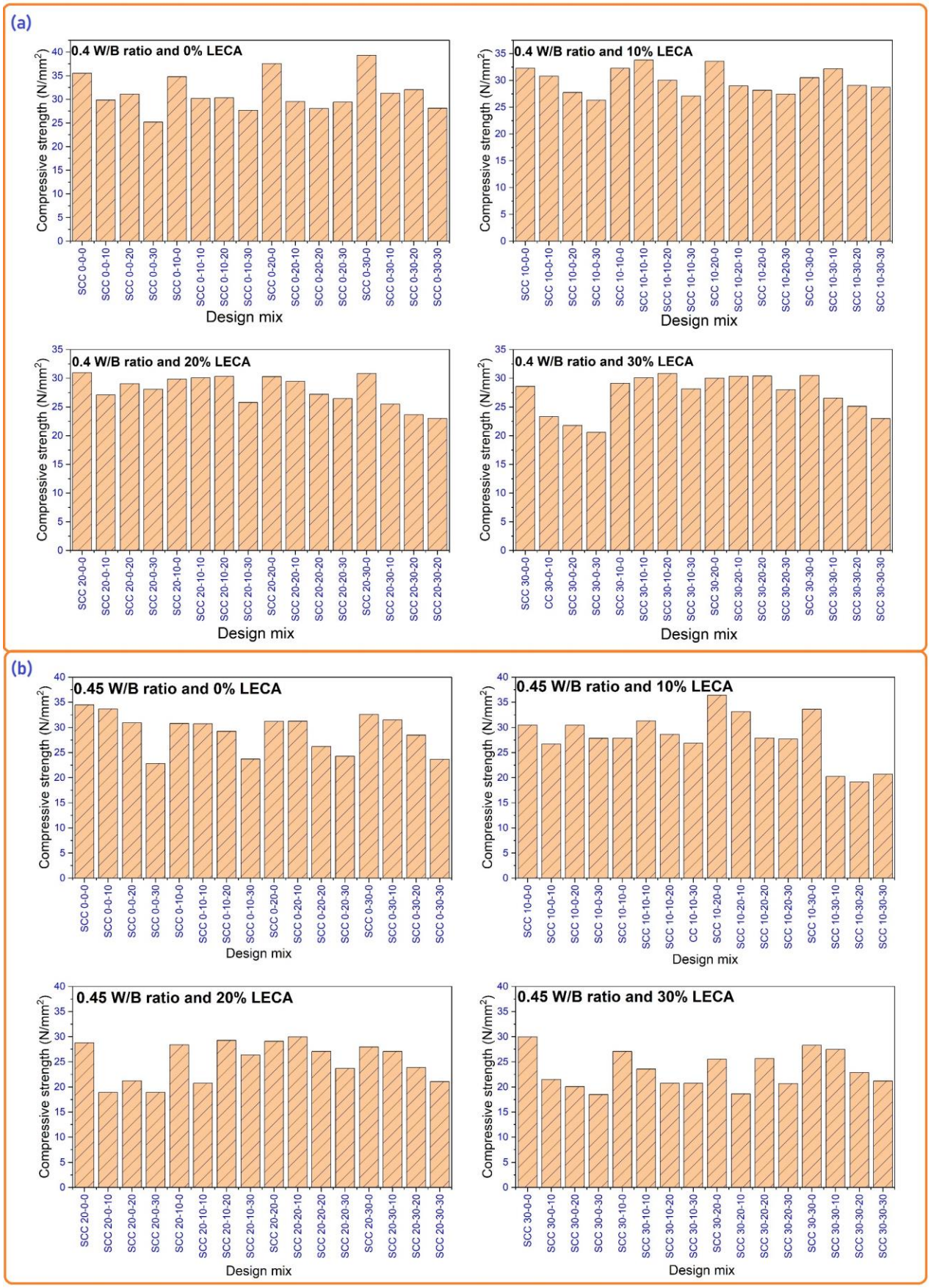


Figure 10. Compressive strengths of SCC mixes: (**a**) 0.4 W/B ratio; (**b**) 0.45 W/B ratio.

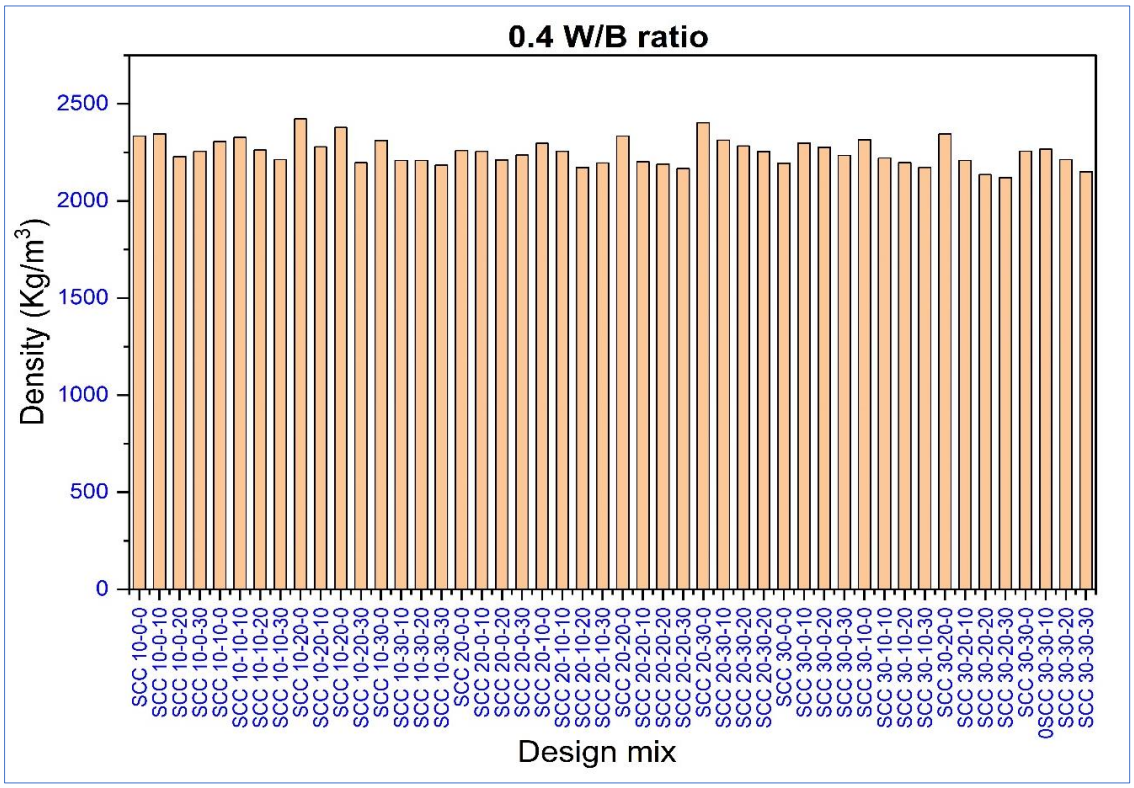


Figure 11. Density of the SCC design mixes at a 0.4 W/B ratio.

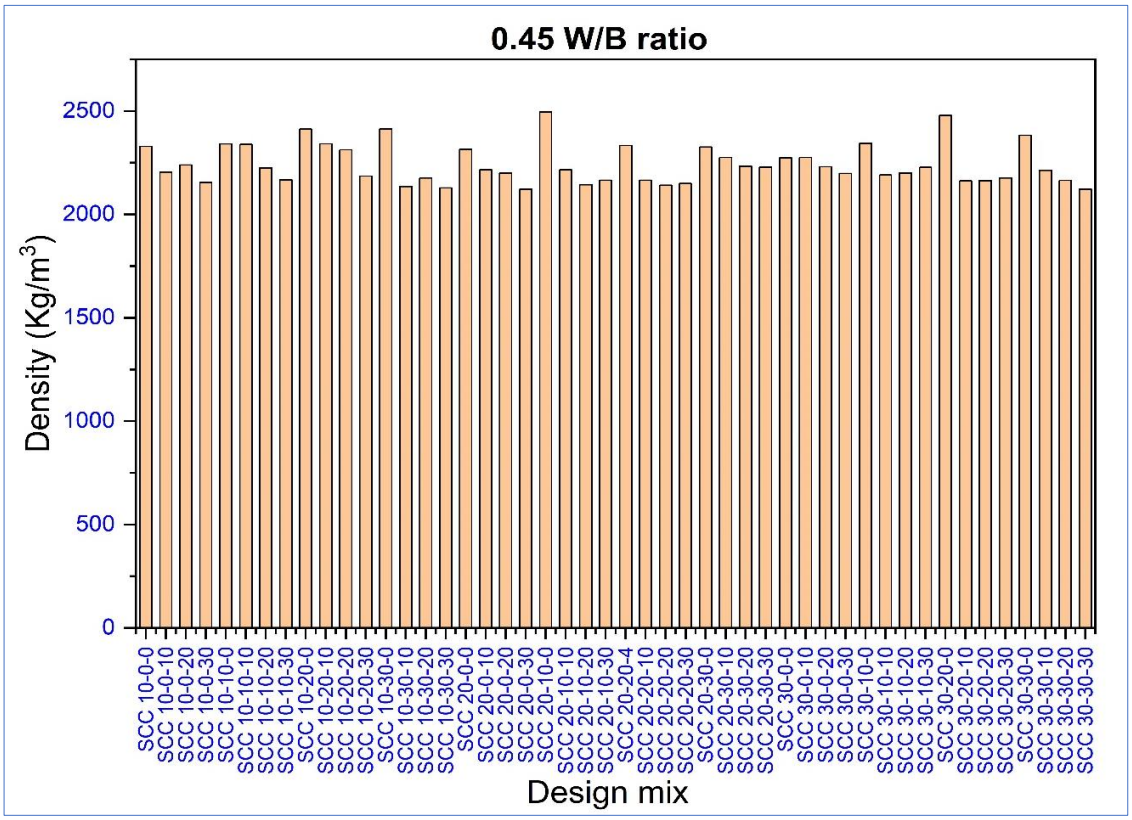


Figure 12. Density of the SCC design mixes at a 0.45 W/B ratio.

4.2. Performance of Machine-Learning Models

Machine-learning models were built to estimate the compressive strength of self-compacting concrete immediately after the results were obtained through experimental work. For this objective, three ML models—ANN, GTB, and CBR—were calibrated and tested. The ML models built were comparatively evaluated in terms of performance metrics, as mentioned in the previous section. Table 10 presents the training and testing performance (in terms of error and efficiency metrics) of the developed ML models. During the testing phase, the CBR provided the CS estimates with the least error when compared with the other two methods, with MAE = 0.5210 (MPa) and RMSE = 0.73955 (MPa). The ANN and GTB estimates had RMSEs (MAEs) that were greater by 146.77% (156.12%) and 59.16% (56.96), respectively, when compared with that of the CBR model. Likewise, the efficiency measures, NNSE and KGE, of the ANN model estimates were 12.79% and 7.19% less than those of the CBR model, respectively. The GTB also underperformed than CBR, with WI lower by 1.4%. Hence, the CBR model predicted the compressive strength of SCC mixes with more accuracy and the least errors.

Table 10. Performance evaluation of ML models using statistical metrics.

MODELS		RMSE (MPa)	MAE (MPa)	SMAPE	NNSE	KGE	WI
ANN	TRAIN	1.8679	1.3715	2.5495	0.8403	0.8970	0.9488
	TEST	1.8249	1.3345	2.4892	0.8469	0.8975	0.9509
GTB	TRAIN	0.9786	0.4003	0.7224	0.9504	0.9011	0.9855
	TEST	1.1770	0.8179	1.5047	0.9300	0.8761	0.9784
CBR	TRAIN	0.1561	0.1189	0.2181	0.9987	0.9918	0.9997
	TEST	**0.73956**	**0.5211**	**0.9649**	**0.9712**	**0.9671**	**0.9923**

From the scatter plots (Figure 13), it can be observed that the CBR model predicted CS more accurately than the other models, with a coefficient of determination R^2 = 0.9703. The violin plot presented in Figure 14 depicts the similarity between the violins of the CBR predictions and the observed CS values. A Taylor diagram (Figure 15) was employed to comparatively evaluate all three model predictions in terms of three indices, namely, the standard deviation, RMSD, and correlation coefficient. It can be observed that the standard deviations of the CBR and ANN model predictions were very close to that of the observed values. The CBR model showed a lower RMSD and higher correlation coefficient compared with the other two models. Based on all three statistical criteria, the CBR model was the best fit for the prediction of the compressive strength of SCC mixes.

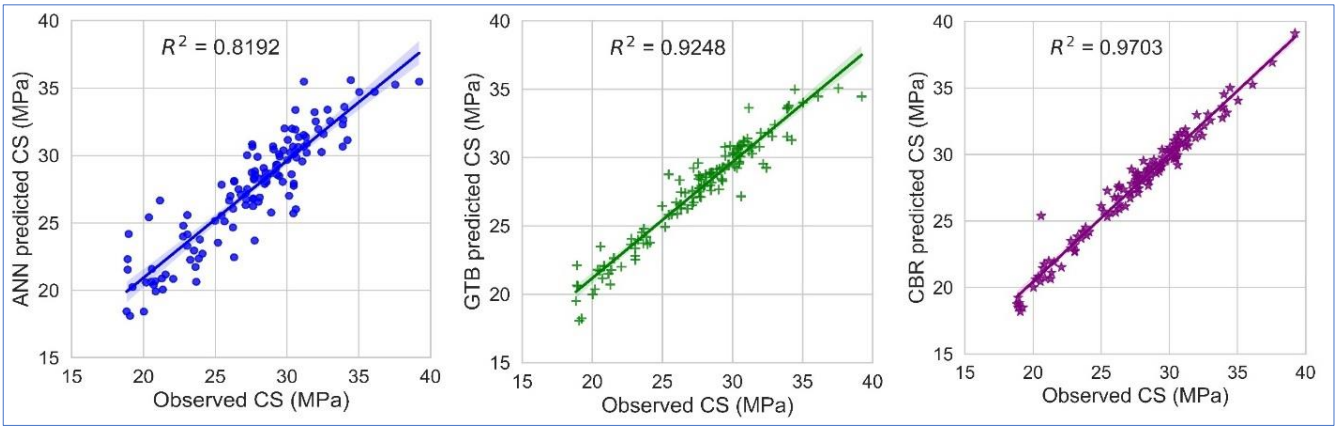


Figure 13. Scatter plots of ANN, GTB, and CBR predictions versus the observed compressive strength of the SCC mixes.

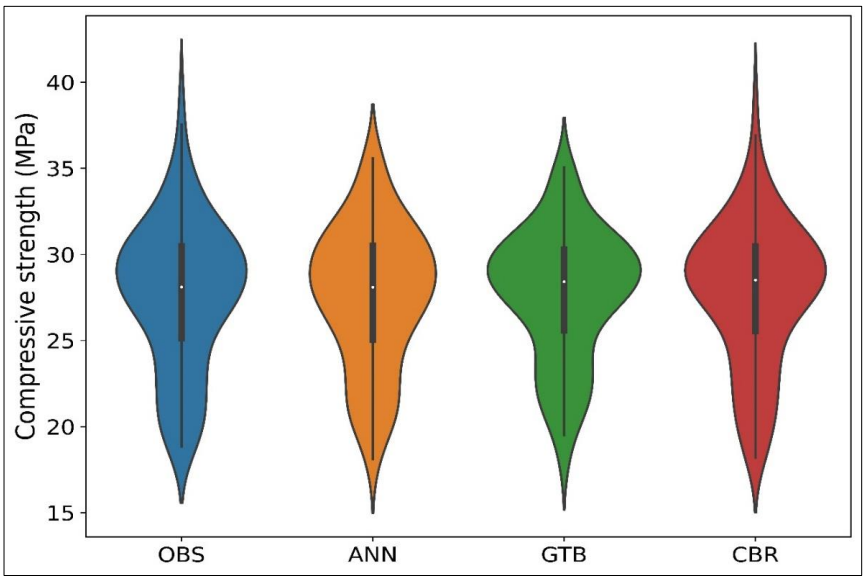


Figure 14. Violin plots of ANN, GTB and CBR predictions.

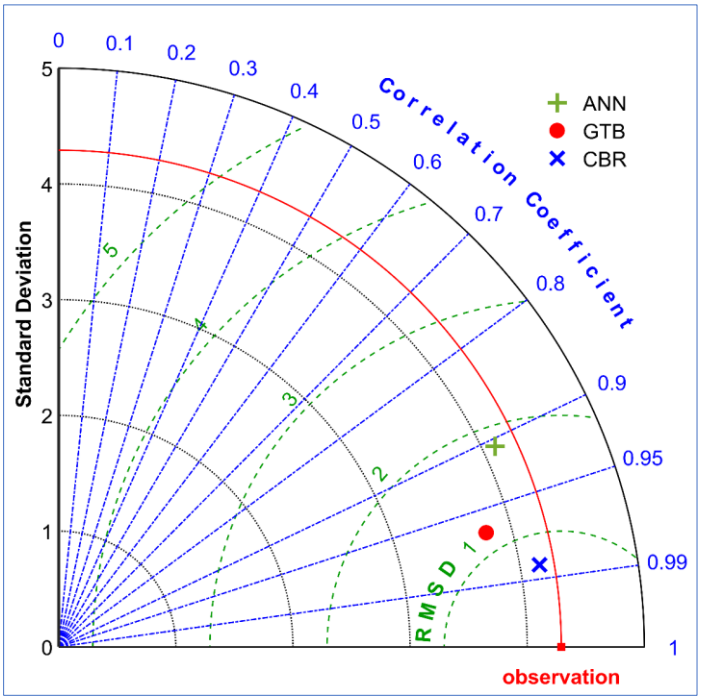


Figure 15. Taylor diagram for comparative evaluation of the models developed.

5. Conclusions

The compressive strength of SCC mixes was experimentally tested and modeled in this study, utilizing artificial neural networks, gradient tree boosting, and CatBoost Regressor. The following are the conclusions arrived at based on the investigation. An increase in compressive strength of about 10.7% was obtained for the SCC mix containing 30% GGBS with a 0.4 W/B ratio and 1.40% superplasticizer. An increase in compressive strength of about 5.59% was obtained for the mix containing 20% GGBS and 10% LECA with a 0.45 W/B ratio and 0.6% superplasticizer. The findings of the experimental study suggest that the ideal LECA, IBMWA, and GGBS replacement percentages for producing SCC are 10%, 20%, and 30%, respectively. However, it is important to note that the optimum material contents and W/B ratio may vary depending on the other mix components and the curing conditions. The inclusion of waste admixtures like IBMWA and GGBS increases the paste

volume. Based on the performance indices of the tested (ANN, GTB, and CBR) models, the CBR model excels in terms of all statistical indices: R^2 = 0.97, MAE = 0.5211 (MPa), RMSE = 0.7395 (MPa), SMAPE = 0.9649%, and NNSE = 0.9712. The CBR approach was more successful than the ANN and GTB methods in predicting the compressive strengths of SCC mixes. A predictive model like CBR can save significant time and energy by providing an accurate compressive strength forecast for mix designs, which can then be used to make decisions.

Supplementary Materials: The following supporting information can be downloaded at https://www.mdpi.com/article/10.3390/su151813621/s1. Table S1: Mix Design; Table S2: DATA used for Modeling.

Author Contributions: N.C.H.G.: conceptualization, methodology, resources, validation, and supervision; K.M.S.: writing—original draft, experimental study; S.R.N.: methodology and writing—editing and review; D.P.: validation, supervision, and visualization. All authors have read and agreed to the published version of the manuscript.

Funding: This research received no external funding.

Institutional Review Board Statement: Not applicable.

Informed Consent Statement: Not applicable.

Data Availability Statement: Data used for modeling are provided in Supplementary Materials. The manuscript along with relevant data is available as a preprint in Research Square. Nahushananda Chakravarthy H G, Karthik M S, Sujay Raghavendra Naganna. Machine-Learning Models for the Prediction of the Compressive Strength of Self-compacting Concrete, 14 March 2023, PREPRINT (Version 1) available at Research Square [https://doi.org/10.21203/rs.3.rs-2667882/v1].

Conflicts of Interest: The authors declare no conflict of interest.

References

1. Okamura, H.; Ozawa, K.; Ouchi, M. Self-compacting concrete. *Struct. Concr.* **2000**, *1*, 3–17. [CrossRef]
2. Domone, P.L. Self-compacting concrete: An analysis of 11 years of case studies. *Cem. Concr. Compos.* **2006**, *28*, 197–208. [CrossRef]
3. Heniegal, A.M. Behavior of underwater self-compacting concrete. *JES. J. Eng. Sci.* **2012**, *40*, 1005–1023. [CrossRef]
4. Moravvej, M.; Rashidi, M. Structural performance of self-compacting concrete. In *Self-Compacting Concrete: Materials, Properties and Applications*; Elsevier: Amsterdam, The Netherlands, 2020; pp. 371–387. [CrossRef]
5. Goodier, C.I. Development of self-compacting concrete. *Proc. Inst. Civ. Eng.-Struct. Build.* **2003**, *156*, 405–414. [CrossRef]
6. Bogas, J.A.; Gomes, A.; Pereira, M.F.C. Self-compacting lightweight concrete produced with expanded clay aggregate. *Constr. Build. Mater.* **2012**, *35*, 1013–1022. [CrossRef]
7. Rashad, A.M. Lightweight expanded clay aggregate as a building material—An overview. *Constr. Build. Mater.* **2018**, *170*, 757–775. [CrossRef]
8. Alqahtani, F.K.; Ghataora, G.; Khan, M.I.; Dirar, S. Novel lightweight concrete containing manufactured plastic aggregate. *Constr. Build. Mater.* **2017**, *148*, 386–397. [CrossRef]
9. Youssf, O.; Hassanli, R.; Mills, J.E.; Elrahman, M.A. An experimental investigation of the mechanical performance and structural application of LECA-Rubcrete. *Constr. Build. Mater.* **2018**, *175*, 239–253. [CrossRef]
10. Adesina, A.; Awoyera, P. Overview of trends in the application of waste materials in self-compacting concrete production. *SN Appl. Sci.* **2019**, *1*, 962. [CrossRef]
11. Sun, C.; Chen, Q.; Xiao, J.; Liu, W. Utilization of waste concrete recycling materials in self-compacting concrete. *Resour. Conserv. Recycl.* **2020**, *161*, 104930. [CrossRef]
12. Al-Oran, A.A.A.; Safiee, N.A.; Nasir, N.A.M. Fresh and hardened properties of self-compacting concrete using metakaolin and GGBS as cement replacement. *Eur. J. Environ. Civ. Eng.* **2022**, *26*, 379–392. [CrossRef]
13. Kavitha, S.; Kala, T.F. Evaluation of Strength Behavior of Self-Compacting Concrete using Alccofine and GGBS as Partial Replacement of Cement. *Indian J. Sci. Technol.* **2016**, *9*, 1–5. [CrossRef]
14. Liu, H.; Chen, W.; Pan, R.; Shan, Z.; Qiao, A.; Drewitt, J.W.; Hennet, L.; Jahn, S.; Langstaff, D.P.; Chass, G.A.; et al. From molten calcium aluminates through phase transitions to cement phases. *Adv. Sci.* **2020**, *7*, 1902209. [CrossRef] [PubMed]
15. Dadsetan, S.; Bai, J. Mechanical and microstructural properties of self-compacting concrete blended with metakaolin, ground granulated blast-furnace slag and fly ash. *Constr. Build. Mater.* **2017**, *146*, 658–667. [CrossRef]
16. Altoubat, S.; Badran, D.; Junaid, M.T.; Leblouba, M. Restrained shrinkage behavior of Self-Compacting Concrete containing ground-granulated blast-furnace slag. *Constr. Build. Mater.* **2016**, *129*, 98–105. [CrossRef]
17. Oner, A.; Akyuz, S. An experimental study on optimum usage of GGBS for the compressive strength of concrete. *Cement Concrete Comp.* **2007**, *29*, 505–514. [CrossRef]

18. Leelavathi, A.; Sudalaimani, K. Study on Self-Compacting Concrete with Sustainable Materials. *Pol. J. Environ. Stud.* **2021**, *30*, 5079–5088. [CrossRef]
19. Hussien, R.M.; Abd El-Hafez, L.M.; Mohamed, R.A.; Faried, A.S. Influence of nano waste materials on the mechanical properties, microstructure, and corrosion resistance of self-compacted concrete. *Case Stud. Constr. Mater.* **2022**, *16*, e00859. [CrossRef]
20. Borhan, T.M.; Abo Dhaheer, M.S.; Mahdi, Z.A. Characteristics of Sustainable Self-compacting Concrete Reinforced by Fibres from Waste Materials. *Arab. J. Sci. Eng.* **2020**, *45*, 4359–4367. [CrossRef]
21. Kaur, H.; Siddique, R.; Rajor, A. Influence of incinerated biomedical waste ash on the properties of concrete. *Constr. Build. Mater.* **2019**, *226*, 428–441. [CrossRef]
22. Altin, S.; Altin, A.; Elevli, B.; Cerit, O. Determination of hospital waste composition and disposal methods: A case study. *Polish J. Environ. Stud.* **2003**, *12*, 251–255.
23. Aubert, J.E.; Husson, B.; Vaquier, A. Use of municipal solid waste incineration fly ash in concrete. *Cement Concrete Res.* **2004**, *34*, 957–963. [CrossRef]
24. Ramesh, B.M.; Vongole, R.M.; Nagraj, Y.; Naganna, S.R.; Sreedhara, B.M.; Mailar, G.; Ramesh, P.S.; Yaseen, Z.M. Valorization of incinerator bottom ash for the production of resource-efficient eco-friendly concrete: Performance and toxicological characterization. *Archit. Struct. Constr.* **2021**, *1*, 65–78. [CrossRef]
25. Hassan, H.F. Recycling of municipal solid waste incinerator ash in hot-mix asphalt concrete. *Constr. Build. Mater.* **2005**, *19*, 91–98. [CrossRef]
26. Manjunath, B.; Di Mare, M.; Ouellet-Plamondon, C.M.; Bhojaraju, C. Exploring the potential use of incinerated biomedical waste ash as an eco-friendly solution in concrete composites: A review. *Constr. Build. Mater.* **2023**, *387*, 131595. [CrossRef]
27. Feng, D.C.; Liu, Z.T.; Wang, X.D.; Chen, Y.; Chang, J.Q.; Wei, D.F.; Jiang, Z.M. Machine learning-based compressive strength prediction for concrete: An adaptive boosting approach. *Constr. Build. Mater.* **2020**, *230*, 117000. [CrossRef]
28. de-Prado-Gil, J.; Palencia, C.; Silva-Monteiro, N.; Martínez-García, R. To predict the compressive strength of self compacting concrete with recycled aggregates utilizing ensemble machine learning models. *Case Stud. Constr. Mater.* **2022**, *16*, e01046. [CrossRef]
29. Yeh, I.-C. Modeling of strength of high-performance concrete using artificial neural networks. *Cement Concrete Res.* **1998**, *28*, 1797–1808. [CrossRef]
30. Lai, S.; Serra, M. Concrete strength prediction by means of neural network. *Constr. Build. Mater.* **1997**, *11*, 93–98. [CrossRef]
31. Asteris, P.G.; Kolovos, K.G.; Douvika, M.G.; Roinos, K. Prediction of self-compacting concrete strength using artificial neural networks. *Eur. J. Environ. Civ. Eng.* **2016**, *20*, s102–s122. [CrossRef]
32. Yaman, M.A.; Elaty, M.A.; Taman, M. Predicting the ingredients of self compacting concrete using artificial neural network. *Alexandria Eng. J.* **2017**, *56*, 523–532. [CrossRef]
33. Zhang, J.; Ma, G.; Huang, Y.; Sun, J.; Aslani, F.; Nener, B. Modelling uniaxial compressive strength of lightweight self-compacting concrete using random forest regression. *Constr. Build. Mater.* **2019**, *210*, 713–719. [CrossRef]
34. Awoyera, P.O.; Kirgiz, M.S.; Viloria, A.; Ovallos-Gazabon, D. Estimating strength properties of geopolymer self-compacting concrete using machine learning techniques. *J. Mater. Res. Technol.* **2020**, *9*, 9016–9028. [CrossRef]
35. Farooq, F.; Czarnecki, S.; Niewiadomski, P.; Aslam, F.; Alabduljabbar, H.; Ostrowski, K.A.; Śliwa-Wieczorek, K.; Nowobilski, T.; Malazdrewicz, S. A Comparative Study for the Prediction of the Compressive Strength of Self-Compacting Concrete Modified with Fly Ash. *Materials* **2021**, *14*, 4934. [CrossRef] [PubMed]
36. Hoang, N.-D. Machine Learning-Based Estimation of the Compressive Strength of Self-Compacting Concrete: A Multi-Dataset Study. *Mathematics* **2022**, *10*, 3771. [CrossRef]
37. Tran, V.Q.; Mai, H.V.T.; Nguyen, T.A.; Ly, H.B. Assessment of different machine learning techniques in predicting the compressive strength of self-compacting concrete. *Front. Struct. Civ. Eng.* **2022**, *16*, 928–945. [CrossRef]
38. Ghorbani, B.; Yaghoubi, E.; Wasantha, P.L.; van Staden, R.; Guerrieri, M.; Fragomeni, S. Machine learning-based prediction of resilient modulus for blends of tire-derived aggregates and demolition wastes. *Road Mater. Pavement Des.* **2023**, *22*, 1–22. [CrossRef]
39. Tang, Y.; Wang, Y.; Wu, D.; Liu, Z.; Zhang, H.; Zhu, M.; Chen, Z.; Sun, J.; Wang, X. An experimental investigation and machine learning-based prediction for seismic performance of steel tubular column filled with recycled aggregate concrete. *Rev. Adv. Mater. Sci.* **2022**, *61*, 849–872. [CrossRef]
40. *IS 8112-1989*; Specification for 43 Grade Ordinary Portland Cement. Bureau of Indian Standards: New Delhi, India, 2013.
41. *IS:383-1970*; Specification for Coarse and Fine Aggregates from Natural Sources for Concrete. Bureau of Indian Standards: New Delhi, India, 2002.
42. *IS:12803-1989*; Methods of Analysis of Hydraulic Cement by X-ray Fluorescence Spectrometer. Bureau of Indian Standards: New Delhi, Indian, 2004.
43. *IS:10262-2019*; Concrete Mix Proportioning—Guidelines. Bureau of Indian Standards: New Delhi, India, 2019.
44. Wang, S.-C. Artificial Neural Network. In *Interdisciplinary Computing in Java Programming*; Springer: Boston, MA, USA, 2003; pp. 81–100. [CrossRef]
45. Wu, Y.; Feng, J. Development and Application of Artificial Neural Network. *Wirel. Pers. Commun.* **2018**, *102*, 1645–1656. [CrossRef]
46. Benardos, P.G.; Vosniakos, G.C. Optimizing feedforward artificial neural network architecture. *Eng. Appl. Artif. Intell.* **2007**, *20*, 365–382. [CrossRef]

47. Gurney, K. *An Introduction to Neural Networks*; CRC Press: London, UK, 2008.
48. Friedman, J.H. Greedy function approximation: A gradient boosting machine. *Ann. Statist.* **2001**, *29*, 1189–1232. [CrossRef]
49. Friedman, J.H. Stochastic gradient boosting. *Comput. Stat. Data. Anal.* **2002**, *38*, 367–378. [CrossRef]
50. Natekin, A.; Knoll, A. Gradient boosting machines, A tutorial. *Front. Neurorobot.* **2013**, *7*, 21. [CrossRef] [PubMed]
51. Prokhorenkova, L.O.; Gusev, G.; Vorobev, A.; Dorogush, A.V.; Gulin, A. *CatBoost: Unbiased Boosting with Categorical Features*; Bengio, S., Wallach, H.M., Larochelle, H., Grauman, K., Cesa-Bianchi, N., Garnett, R., Eds.; NeurIPS: Montréal, QC, Canada, 2018; pp. 6639–6649. Available online: https://proceedings.neurips.cc/paper/2018/file/14491b756b3a51daac41c24863285549-Paper.pdf (accessed on 30 December 2022).
52. Hancock, J.T.; Khoshgoftaar, T.M. CatBoost for big data: An interdisciplinary review. *J. Big Data* **2020**, *7*, 94. [CrossRef]
53. Mohamed, O.A.; Najm, O.F. Compressive strength and stability of sustainable self-consolidating concrete containing fly ash, silica fume, and GGBS. *Front. Struct. Civ. Eng.* **2017**, *11*, 406–411. [CrossRef]
54. Dolatabad, Y.A.; Abolpour, B.; Tazangi, M.A.J. Investigating effects of Nano particles of silica on the properties of self-compacting concrete containing Perlite, Leca, and Scoria light weight aggregates. *Arab. J. Geosci.* **2021**, *14*, 862. [CrossRef]

Disclaimer/Publisher's Note: The statements, opinions and data contained in all publications are solely those of the individual author(s) and contributor(s) and not of MDPI and/or the editor(s). MDPI and/or the editor(s) disclaim responsibility for any injury to people or property resulting from any ideas, methods, instructions or products referred to in the content.